Biomaterials 302 (2023) 122363

Contents lists available at ScienceDirect

Biomaterials

journal homepage: www.elsevier.com/locate/biomaterials

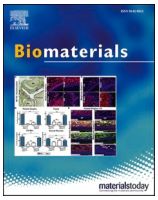

Conductive electrospun polymer improves stem cell-derived cardiomyocyte function and maturation

Gisselle Gonzalez [a], Aileena C. Nelson [a], Alyssa R. Holman [b], Alexander J. Whitehead [a], Erin LaMontagne [a], Rachel Lian [a], Ritwik Vatsyayan [c], Shadi A. Dayeh [c], Adam J. Engler [a,b,d,*]

[a] Shu Chien-Gene Lay Department of Bioengineering, La Jolla, CA, 92093, USA
[b] Biomedical Sciences Graduate Program, La Jolla, CA, 92093, USA
[c] Department of Electrical and Computer Engineering, University California San Diego, La Jolla, CA, 92093, USA
[d] Sanford Consortium for Regenerative Medicine, La Jolla, CA, 92037, USA

ARTICLE INFO

Keywords:
poly(3,4-ethylenedioxythiophene):polystyrene sulfonate (PEDOT:PSS)
poly(vinyl) alcohol (PVA)
Desmoplakin
Sarcomere organization
Calcium handling
FluoVolt

ABSTRACT

Despite numerous efforts to generate mature human pluripotent stem cell-derived cardiomyocytes (hPSC-CMs), cells often remain immature, electrically isolated, and may not reflect adult biology. Conductive polymers are attractive candidates to facilitate electrical communication between hPSC-CMs, especially at sub-confluent cell densities or diseased cells lacking cell-cell junctions. Here we electrospun conductive polymers to create a conductive fiber mesh and assess if electrical signal propagation is improved in hPSC-CMs seeded on the mesh network. Matrix characterization indicated fiber structure remained stable over weeks in buffer, scaffold stiffness remained near *in vivo* cardiac stiffness, and electrical conductivity scaled with conductive polymer concentration. Cells remained adherent and viable on the scaffolds for at least 5 days. Transcriptomic profiling of hPSC-CMs cultured on conductive substrates for 3 days showed upregulation of cardiac and muscle-related genes versus non-conductive fibers. Structural proteins were more organized and calcium handling was improved on conductive substrates, even at sub-confluent cell densities; prolonged culture on conductive scaffolds improved membrane depolarization compared to non-conductive substrates. Taken together, these data suggest that blended, conductive scaffolds are stable, supportive of electrical coupling in hPSC-CMs, and promote maturation, which may improve our ability to model cardiac diseases and develop targeted therapies.

1. Introduction

Since the early efforts in differentiating human pluripotent stem cells into cardiomyocytes (hPSC-CMs), their potential to study various cardiovascular diseases and their use as a therapeutic for diseases has been greatly explored [1–3]. While initial studies aimed to differentiate hPSC-CMs in two-dimensional (2D) monolayers and maximize cell population purity [4,5], current efforts strive to generate more mature cells by recapitulating the complexity of native cardiac tissue [6,7]. Previous studies indicate that hPSC-CM maturation requires paracrine signaling between various cell types that compose cardiac tissue [8], a tissue-relevant microenvironment conducive to cellular communication [9], and more recently, electrical and mechanical stimulation [10]. However, despite many efforts to achieve mature cells, hPSC-CMs remain immature, exhibit poor sarcomere organization important for contractility, experience asynchronous contractions, and fail to replicate metabolic activity levels of native cardiomyocytes [6].

Biomaterials are being explored as methods to address these problems and enhance overall cardiac tissue maturation. Most biomaterials create an insulating environment, which may impede electrical propagation, but recently, conductive materials [1] have been substituted to improve electrical maturation and signal propagation between cells. Polypyrrole (PPy) and polyaniline (PANI) are among the most studied conductive polymers [2–6], but these materials are difficult to disperse in an aqueous environment and are cytotoxic, raising concerns for their long-term use in physiological conditions [7]. In contrast, poly(3,4-ethylenedioxythiophene) poly(styrene sulfonate) (PEDOT:PSS) has recently been shown to be conductive in an aqueous environment [7] whereas PPy and PANI are not. PEDOT:PSS biocompatibility may be more limited than other PEDOT derivatives [8,9], but when blended with other polymers, such as poly(vinyl) alcohol (PVA) and a poly (ethylene glycol) (PEG)-based crosslinker [10], PEDOT:PSS may exhibit

* Corresponding author. Shu Chien-Gene Lay Department of Bioengineering, La Jolla, CA, 92093, USA.
E-mail address: aengler@ucsd.edu (A.J. Engler).

https://doi.org/10.1016/j.biomaterials.2023.122363
Received 2 June 2023; Received in revised form 16 October 2023; Accepted 20 October 2023
Available online 21 October 2023

improved chemical stability and biocompatibility. Likewise, the addition of synthetic biocompatible polymers can further tune mechanical properties, such as degradation rate and stiffness, of PEDOT:PSS products to better mimic the native cardiac tissue environment. Alongside composition, these materials can be configured as nanofibers by electrospinning [19] to better simulate the fibrous extracellular matrix (ECM) structure of native tissues. By electrospinning blends of biocompatible and conductive polymers, a tunable, conductive environment for hPSC-CM maturation and function may be possible.

Cardiomyocytes in the heart exist in three-dimensional layers, interrupted by sporadic cardiac fibroblasts, immune cells, blood vessels, and ECM, among other constituents. A conductive polymer may be able to propagate signals and synchronous contraction even in sub-confluent monolayers of hPSC-CMs as would occur between layers in the heart. To assess the degree to which this was possible, we first evaluated the material properties and biocompatibility of electrospun PEDOT:PSS/PVA scaffolds. In hPSC-CMs, conductive substrates increased expression of cardiac related genes as well as the localization and organization of junction and structural proteins, such as desmoplakin (DP) and α-actinin, respectively. Higher cardiac gene expression and improved structure led to more coordinated calcium handling, even in sub-confluent hPSC-CM layers. Prolonged hPSC-CM culture on conductive scaffolds demonstrated higher cell retention and action potential intensities, overall suggesting that conductive polymer networks may improve function and contribute to the maturity of hPSC-derived cardiac tissue constructs.

2. Materials and methods

2.1. Preparation of PVA/PEDOT:PSS/PEGDE solutions

PVA (Sigma-Aldrich, 363146) was dissolved in deionized (DI) water at a 20 % (w/v) at 130 °C under magnetic stirring for 3 h. Poly(ethylene glycol) diglycidyl ether (PEGDE, Sigma-Aldrich, 475696) was mixed with PEDOT:PSS 1.3 % wt. dispersion in water (Sigma-Aldrich, 483095) at a 3 % (w/v) concentration as described by Solazzo et al. [10]. The 3 % PEGDE/PEDOT:PSS solution was vortexed for 30 s, sonicated for 30 min, and syringe filtered with a 0.45 μm filter (Corning, 431225) to remove aggregates. The resulting solutions were combined to create base 8 % (w/v) PVA solutions with 0 %, 3.25 %, 6.5 %, and 9.75 % mass to mass ratio solutions of PEDOT:PSS to PVA. A mass-matched solution of 11 % (w/v) PVA was created to match the polymer mass of the 9.75 % solution. Solutions were vortexed for 1 h to form a homogeneous mixture and desiccated for 1 h to remove air bubbles.

2.2. Composite PVA/PEDOT:PSS/PEGDE electrospun scaffold fabrication

An Inovenso Nanospinner (KTP700 Basic) electrospinner was utilized for scaffold fabrication at 0.5–0.75 mL/h flow rate, 20 cm working distance, 33 kV applied voltage, and 30 % humidity with a 0.8 mm nozzle for a total of 0.1 mL solution spun per session. Scaffolds were collected on 18 mm coverslips (Fisherbrand, 12545100) for scanning electron microscopy (SEM), atomic force microscopy (AFM), and biological experiments and on 24 × 40mm coverslips (Fisherbrand, 12545D) for conductivity measurements. To crosslink the polymers, scaffolds were placed in a glass chamber (Chemglass, AF-0556) in the presence of 0.2 M glutaraldehyde, subjected to vacuum for 15 s, and placed in an oven at 80 °C for either 15 or 30 min. After crosslinking, scaffolds were washed three times for 30 min with a 1 % (w/v) glycine solution to remove unreacted glutaraldehyde, followed by three 10-min washes in DI water [11]. Crosslinked scaffolds were dried at room temperature overnight prior to use.

2.3. Scaffold degradation and fiber morphology

After either 15 or 30 min of crosslinking, 8 % w/v PVA electrospun scaffolds were incubated in DPBS (1X) (Gibco, 14190-144) at 37 °C over 4 weeks. Scaffolds containing 9.75 % PEDOT:PSS/PVA crosslinked at 30 min were also incubated to investigate the degradation of conductive scaffolds. Scanning electron microscopy (SEM) images of scaffolds immediately before and after crosslinking, as well as after 1, 2, or 4 weeks of incubation were obtained on a Zeiss Sigma 500 SEM. The scaffolds were mounted on carbon-taped standard aluminum stubs and sputter coated with iridium to reduce electron charging on the sample surface. A working accelerating voltage of 3 kV and an objective aperture of 30 μm were utilized for all samples. Three images per scaffold at each timepoint were obtained. SEM images obtained at 10 k magnification were analyzed on ImageJ to determine the average electrospun fiber diameter over time. Three images per scaffold and 10 fibers per image were measured. In instances where the fibers annealed and formed a film, the fiber diameter was not measured.

2.4. Bulk stiffness

Bulk stiffness after 30 min of crosslinking was measured using an Oxford Instruments MFP-3D Bio atomic force microscope (AFM). Scaffolds with an 8 % PVA base containing 0 %, 3.25 %, 6.5 % and 9.75 % PEDOT:PSS/PVA as well as a mass-matched 11 % PVA scaffold were soaked for 1 h in DPBS prior to AFM and maintained in DPBS during measurements. A silicon nitride cantilever with a 45 μm polystyrene bead tip and 0.03 N/m stiffness (Novascan) was utilized with a scan rate of 8 kHz, 1 nN trigger force, 2 μm/s velocity, and 3 μm force distance. Three force maps of 20 × 20μm with a total of 20 points per force map were obtained per sample, with 4 scaffolds per group. Force maps were analyzed by fitting a Hertz model to the curves [12].

2.5. Conductivity measurements

Transfer length method (TLM) measurements were performed to determine the sheet conductivity. Autodesk AUTOCAD was used to create a software mask, which was patterned on polyethylene terephthalate (PET) tape using a Universal Laser Systems VLS3.60DT laser cutter to create a shadow mask for metal deposition directly on electrospun scaffolds via electron beam (e-beam) evaporation. 50 nm thick gold (Au) rectangular contacts with 1 cm width were deposited on the scaffolds with inter-contact spacings of 500, 1000, 2000, 3000, 4000 and 5000 μm. Current-voltage measurements for inter-contact resistance evaluation were conducted using an Agilent B1500A Semiconductor Device Analyzer. In TLM, the resistance between contact pairs provides a measure of the contact resistance between the Au and the scaffolds (independent of inter-contact spacing) and total scaffold film resistance between the contacts (linearly dependent on inter-contact spacing). The sheet resistance may be calculated from the slope of the line-fit when plotting resistance against inter-contact spacing from:

$$slope = \frac{R_{sh}}{W} \tag{1}$$

where R_{sh} is the sheet resistance ($\Omega\ sq^{-1}$) and W is the Au contact width [13,14]. The final material conductivity was calculated by:

$$\sigma = \frac{1}{R_{sh} \bullet t} \tag{2}$$

where σ is conductivity (S/cm^2) and t is the electrospun scaffold thickness. To measure thickness, scaffolds were hydrated, cut to create a height difference between the scaffold and glass substrate. Dried scaffolds were measured via a Dektak XT Stylus Profilometer (Bruker) with a 12.5 μm stylus tip radius, 3 mg stylus force, and 6.5 μm range.

2.6. Scaffold sterilization and NIH/3T3 cell culture

Scaffolds containing increasing PEDOT:PSS suspended on 18 mm coverslips were crosslinked for 30 min and sterilized under UV for 1 h on either side, transferred to 12 well plates, and washed with sterile DPBS three times to remove debris. A 0.1 % (w/v) gelatin-coated glass substrate was used as a positive control in all experiments, while an 11 % PVA scaffold was used as a mass-matched control. NIH/3T3 embryonic mouse fibroblasts were seeded at a concentration of 20,000 cells per well. Media composed of DMEM (Dulbecco's Modified Eagle Media; Gibco, 11966025), 10 % v/v fetal bovine serum (FBS) (Omega Scientific, NC0471611), and 1 % v/v penicillin/streptomycin (Gibco, 15070063) was changed daily.

2.7. Cell viability assays

Material cytotoxicity was determined via a LIVE/DEAD Viability/Cytotoxicity kit (Invitrogen, L3224). Cells adhered onto each substrate for 24–120 h, were washed with DPBS, then incubated in 2 μM calcein-AM and 4 μM ethidium-homodimer-1in DPBS for 30 min at room temperature. Scaffolds were inverted onto a 35 mm glass bottom culture dish (MatTek, P35G-0-20-C) and sealed with Parafilm to prevent solution evaporation. A Nikon Eclipse Ti microscope with a Yokogawa CSU-X1 confocal attachment were used to image the percentage of live and dead cells. ImageJ was used to quantify the percentage of live to dead cells at 1 and 5 days after cell seeding. Alternatively, cells were stained with Ki67 (1:800, Invitrogen, 14-5698-82) at day 5 to mark nuclei for dividing cells and quantified similarly to the live-dead stain using ImageJ.

In addition to the live/dead assay, a resazurin cell viability assay (Biotium, 30025) was performed on NIH/3T3s. Cells were allowed to adhere for 4 h, then incubated in media containing 10 % (v/v) resazurin. After 4 h of incubation, 100 μL of media per sample was transferred to a 96 well plate. The fluorescence was read using a microplate reader (ex./em. 560/590, BioTek Synergy 4). Cell-free scaffolds were also incubated in 10 % resazurin and used as blanks to subtract any background fluorescence from the scaffolds. Media was changed and the assay repeated on days 1, 3, and 5 after initial cell attachment.

2.8. hPSC-CM differentiation and cell seeding

RUES2 hPSCs were expanded on Matrigel-coated 6-well plates (Corning, CLS354234) in mTeSR 1 media (Stemcell Technologies, 85850) with daily changes. Cells were passaged at 85–90 % confluency at 1:6 by incubating for 4 min in Versene (Gibco, 15040066), lifting with a cell scraper, and resuspending in media supplemented with 5 μM Y-27632 dihydrochloride (LC Laboratories, Y-5301). To produce hPSC-CMs, the GiWi cardiac differentiation protocol was employed [15].

After 50 days of cardiac differentiation, the resulting hPSC-CMs were seeded on 8 % PVA scaffolds containing 0 %, low (3.25 %), and high (9.75 %) concentrations of PEDOT:PSS suspended on 18 mm coverslips as well 0.1 % gelatin-coated glass 18 mm coverslips in 12-well plates. hPSC-CMs were dissociated in 0.5 mL collagenase IV (4 mg/mL, Gibco, 17104-019) for 50 min at 37 °C, followed by 25 min in 0.5 mL 0.25 % Trypsin-EDTA (Gibco, 25200) at 37 °C. Cells were quenched in RPMI + B27 with insulin +20 % FBS v/v + 5 μM Y-27632 dihydrochloride and centrifuged at 400 g for 10 min. hPSC-CMs were resuspended in the quenching media and seeded at 10^4 (sub-confluent monolayer) or 10^6 (monolayer) cells per well (4×10^3 or 4×10^5 cells/cm^2, respectively).

2.9. RNA isolation, sequencing and analysis

hPSC-CMs on 8 % PVA or conductive scaffolds were dissociated with 0.5 mL 0.25 % Trypsin-EDTA and pelleted centrifugation at 400*g* for 5 min. The cells were resuspended in DPBS, re-pelleted, and lysed with 1 mL QIAzol (Qiagen, 79306) for 5 min. Chloroform was added 1:5 to QIAzol, shaken for 15 s, and incubated for 3 min. The samples were centrifuged for 10 min at 15,000 RPM and 4 °C (Eppendorf, Centrifuge 5452 R) and the aqueous phase containing the RNA was transferred to new tubes. An equal volume of isopropanol was added, and the samples were allowed to rest for 10 min, followed by a 10-min centrifugation at 15,000 RPM at 4 °C. The supernatant was then removed and the RNA pellet was resuspended in 1 mL of cold 75 % molecular grade ethanol in diethylpyrocarbonate (DEPC) water. The samples were re-pelleted at 15,000 RPM at 4 °C, decanted, and resuspended in 100 μL of DEPC water. An RNeasy Mini kit (Qiagen, 74104) was used to purify the RNA following the manufacturer's protocol. The final RNA concentration was measured by a Nanodrop spectrophotometer and the samples were stored at −80 °C for further processing.

Bulk RNA sequencing was performed by the Institute for Genomic Medicine at UC San Diego. Total RNA integrity was assessed via an Agilent TapeStation 4200. Samples with an RNA Integrity Number (RIN) above 8.0 were prepared using the Illumina Total RNA Prep (Ribodepletion) and sequenced with the Illumina NovaSeq 6000 with paired end reads (PE100). Quality of sequencing data was assessed using FASTQC [16]. Reads were aligned to the human reference genome hg38 using STAR [17] and gene counts were determined using featureCounts [18]. Log_2 fold changes of differentially expressed genes (DEGs) were determined with DESeq2 [19] via a paired model of non-conductive versus conductive substrates and including biological replicates as a covariate. Top DEGs were filtered with a log_2 fold change greater than or equal to 0.25 and p-value less than or equal to 0.05 and used to construct a volcano plot via EnhancedVolcano [20], an MA plot via ggpubr's 'ggmaplot' function [21], as well as to determine gene ontology(GO) terms via g:Profiler [22]. For generating a principal component analysis (PCA) plot and heatmap, normalization of sequencing data into log_2 counts per million (cpm) was performed with edgeR [23]. Batch effect corrections due to biological replicates was performed with the sva package's 'ComBat' function [24] after averaging technical replicates. Normalized data with batch correction were used to generate a PCA plot via ggplot [25] and heat map via pheatmap [26]. Raw RNA-sequencing was deposited and is accessible in NCBI under the Gene Omnibus Express number GSE226541.

2.10. hPSC-CM immunofluorescent assays

After 50–70 days in culture, hPSC-CMs were allowed to adhere to conductive electrospun scaffolds and a glass control for 3 days prior to fixation with 3.7 % paraformaldehyde (Fisher Scientific, O4042-500) in DPBS with calcium and magnesium (Corning, 20-030-CV) for 15 min at room temperature. Cells were permeabilized in 0.5 % (v/v) Triton X-100 (Fisher Bioreagents, BP151-100) for 10 min and blocked for 1 h in DPBS with calcium and magnesium containing 2 % w/v bovine serum albumin (BSA, Goldbio, A-420-10) and 0.1 % (v/v) Triton X-100. hPSC-CMs were incubated in either desmoplakin 1/2 (DP) (1:200, Biorad, 2722–5204) primary antibodies to determine cell-cell mechanical coupling, or α-actinin (1:800, Sigma-Aldrich, A7811) primary antibodies for detecting sarcomere organization for 2 h at room temperature in the blocking buffer. Samples were then incubated in AlexaFluor 488 conjugated donkey anti-mouse (1:1000, Invitrogen, A21202) antibody and rhodamine-phalloidin (1:500, Biotium, 00027) for 2 h at room temperature. Samples were finally incubated in Hoechst 33342 in DI water (1:2000, Invitrogen, H3570) for 15 min at room temperature, mounted on slides with Fluoromount-G (Southern Biotech, 0100-01), and allowed to dry overnight prior to immunofluorescent (IF) imaging. A Zeiss LSM 780 confocal microscope with a 63× oil objective and Nikon Eclipse Ti microscope with a Yokogawa CSU-X1 confocal attachment and a 60× water objective were used to image DP and α-actinin.

DP intensity analysis was performed with ImageJ with brightness and contrast adjusted to overexpose the area of the image with cells and then converted to an inverted binary image. The mask was applied to the original DP channel such that the mean pixel intensity was only

quantified in the region of the image with hPSC-CMs. For sarcomere organization, images were converted into 8-bit, split into individual channels, and the background was removed from the α-actinin channel. A grid was placed over the image and a random number generator was used to select regions of interest for analysis. Each region was analyzed using an open-source MATLAB script [27] that produces a normalized organization index.

2.11. Calcium handling

hPSC-CMs were seeded at sub-monolayer and monolayer densities on electrospun scaffolds with increasing PEDOT:PSS concentration. hPSC-CMs were further seeded on 0.1 % gelatin coated 35 mm glass bottom culture dishes. After 3 days of attachment, scaffolds were transferred to 35 mm glass bottom culture dishes and incubated with 2 μM fluo-4 AM ester (Biotium, 50018) in RPMI + B27 with insulin for 15 min at 37 °C in the dark. After 15 min, the scaffolds were inverted in the dish and imaged using a Nikon Eclipse Ti microscope with a Yokogawa CSU-X1 confocal attachment and a 60× water objective. Five videos per sample across 3–4 biological replicates were captured for 30 s with 100 ms intervals for a total of 301 frames. In ImageJ, the rotated rectangle tool was used to select 1-pixel wide sections perpendicular to the calcium flux on individual cells. The selection was duplicated and converted into an orthogonal XZ view. Two sections per cell were analyzed. The XZ projections were saved and analyzed using a custom MATLAB script, which is available via Github (https://github.com/englea52/PEDOT_PSS).

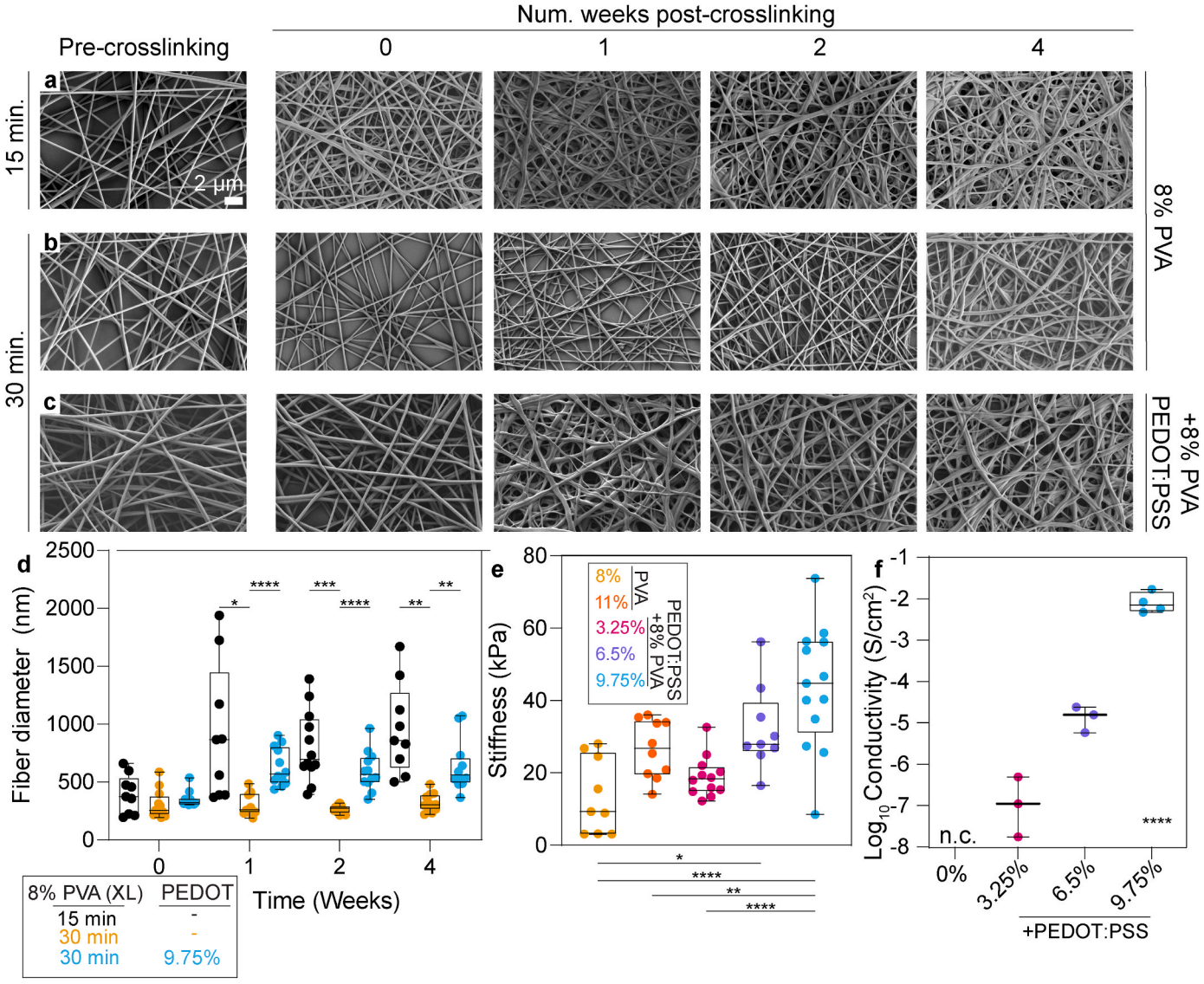

Fig. 1. Physical characterization of electrospun scaffolds. (a) SEM images of 8 % PVA electrospun scaffolds incubated in DPBS 4 weeks post-crosslinking with glutaraldehyde vapor for 15 min, (b) 30 min, and (c) 30 min with 9.75 % PEDOT:PSS/PVA. Scale bar = 2 μm. (d) After 4 weeks of incubation, 8 % PVA crosslinked for 15 min had a median fiber diameter of 828.04 nm (n = 3 scaffolds for week 0, 1, 4; n = 4 scaffolds for week 2; 3 average measurements per scaffold), while 8 % PVA crosslinked for 30 min had a median fiber diameter of 302.7 nm and 560.1 nm with PEDOT:PSS (n = 4 scaffolds per timepoint, 3 average measurements per scaffold). (e) Bulk stiffness (kPa) of PVA-only (8 % and 11 %) and 8 % PVA with PEDOT:PSS (3.25 %, 6.5 %, and 9.75 % mass ratio) electrospun scaffolds crosslinked for 30 min measured by AFM. Median stiffness values of 8 % PVA, 11 % PVA, 3.25 %, 6.5 %, and 9.75 % were 9.30, 26.68, 18.36, 27.91, and 44.76 kPa, respectively (n = 4 scaffolds per condition; 1 point represents 1 force map). (f) Conductivity measurements of 8 % PVA electrospun scaffolds containing 0–9.75 % PEDOT:PSS measured by TLM. Median conductivity values of 3.25 %, 6.5 %, and 9.75 % were 1.09×10^{-7}, 1.57×10^{-5}, and 7.00×10^{-3} S/cm^2, respectively. Each point indicates one scaffold (n.c. indicates not conductive, n = 2). Statistical significance was determined via a mixed-effects analysis (d), a one-way ANOVA with Tukey's multiple comparison test (e), or just a one-way ANOVA (f).

2.12. FluoVolt imaging

hPSC-CMs were seeded at monolayer densities on electrospun scaffolds with increasing PEDOT:PSS concentration and gelatin-coated glass. After 7 days of attachment, scaffolds were incubated in FluoVolt membrane potential dye (Invitrogen, F10488) in Tyrode's solution (Thermo Scientific Chemicals, J67593-K2) following the manufacturer's protocol. Briefly, scaffolds were washed twice with Tyrode's solution and incubated with FluoVolt loading solution at 37 °C in the dark. Scaffolds were then washed twice in Tyrode's solution, inverted onto a glass bottom well plate (Cellvis, P24-0-N), and maintained in fresh Tyrode's solution for imaging. Samples were imaged on an Andor Dragonfly spinning disk confocal microscope. Five videos per sample across 3 biological replicates were captured for 20 s with 2.5 ms intervals. In ImageJ, the rotated rectangle tool was used to select 1-pixel wide sections across several regions of interest (ROIs) in each video (5 ROIs per monolayer or 1 ROI per cell cluster in instances lacking a monolayer). ROIs were analyzed similarly to calcium handling sections using our custom MATLAB script.

2.13. Statistical analysis

The respective statistical tests and n numbers are described in the figure legends. The following statistical significance cut off was applied: $p > 0.05$, *$p < 0.05$, **$p < 0.01$, ***$p < 0.01$, ****$p < 0.0001$. Data expressed as box-and-whisker plots show all points with the whisker ends corresponding to minimum and maximum values. All other values are expressed as mean ± SD. Statistical analyses were performed using GraphPad Prism Software v9.0.

3. Results and discussion

3.1. Characterization of PEDOT:PSS/PVA electrospun scaffolds

To create fibrillar conductive scaffolds, we blended and electrospun PVA and PEDOT:PSS and crosslinked the resultant scaffolds for either 15 or 30 min to prevent PVA dissolution (Fig. 1a–b). PVA scaffolds remained fibrous for up to 4 weeks in solution with 30 min of crosslinking, although the addition of 9.75 % PEDOT:PSS to the same scaffold (Fig. 1c) led to an initial increase in fiber diameter compared to PVA-only scaffolds (Fig. 1d). However, conductive fiber diameters remained within the range of fiber diameters within collagen type I gels [28]. Since PVA scaffolds crosslinked at 30 min experienced the least amount of fiber annealing over time, subsequent experiments were performed on these scaffolds.

Along with scaffold structure, material stiffness is well-known to affect stem cell fate and cell spreading [29,30]; hence, we also assessed electrospun scaffolds stiffness. Bulk stiffness scaled with PEDOT:PSS concentration (Fig. 1e) and stiffness values spanned a range consistent with normal cardiac muscle [31]. The large variance observed in stiffness values may reflect the random nature of the PVA mesh from electrospinning, despite using larger AFM probes for measurement. Since hPSC-CMs are electrically active cells and given the anisotropic structure of electrospun scaffolds [32], we measured PEDOT:PSS/PVA scaffold conductivity using TLM, which uses a network of variable length resistors made by the scaffolds to evaluate contact resistance and sheet resistance [13,14] (Fig. S1). 8 % PVA was non-conductive, i.e., insulating, whereas conductivity increased substantially with PEDOT:PSS concentration, up to 7×10^{-3} S/cm^2 (Fig. 1f). These data suggest scaffold properties are consistent and mimic physiologically relevant conditions when crosslinked at 30 min and additional electrically conductive properties are achievable with the incorporation of PEDOT:PSS.

3.2. PEDOT:PSS/PVA biocompatibility

To ensure that hPSC-CM results were not affected by variable attachment, proliferation, or survival, we first determined how a non-conductive cell type, e.g., NIH/3T3 fibroblasts, behaved on the electrospun scaffolds. Cells preferentially adhered to conductive scaffolds and glass versus non-conductive scaffolds (Fig. 2a–c) but remained >90 % viable on all substrates. Given that 8 % PVA scaffolds are thinner due to their lower total polymer mass compared to our highest PEDOT:PSS percentage of 9.75 %, we introduced an 11 % PVA scaffold as a mass-matched control to the 9.75 % condition. Independent of mass, however, cell attachment remained higher on conductive scaffolds compared to both non-conductive controls (Fig. 2d). To quantitatively assess proliferation, we also monitored metabolic changes over five days by resazurin reduction. Given higher initial cell attachment on the conductive scaffolds compared to PVA-only scaffolds (Fig. 2a–c), fluorescence intensity signal was greater on conductive scaffolds at day 0 and remained higher on conductive scaffold over the time course (Fig. 2e). Gelatin-coated glass had the highest attachment, perhaps due to the presence of ECM proteins, which were purposefully excluded from the electrospun scaffold samples to directly assess cell adhesion to the fiber and not a matrix coating. Yet, serum proteins are classically known to deposit on electrically conductive substrates [33], hence the enhanced cell binding to PEDOT:PSS versus PVA could be due to non-specific serum protein binding. Resazurin reduction is affected by initial adhesion, hence we also stained cells for the proliferation marker Ki67, which enables single cell assessment of proliferation. While we found differences with cells cultured on gelatin-coated glass, there were no differences in proliferation between scaffolds of varying PVA and PEDOT:PSS (Fig. 2f). Similarly high levels of cell adhesion and proliferation to PEDOT:PSS fibers and substrates have been reported with other mouse and human fibroblast lines relative to control fibers or surfaces [34,35], suggesting that conductive substrates have low cytotoxicity and support cell adhesion and proliferation.

3.3. Conductive scaffolds upregulate cardiac-related genes, improve cytoskeletal structures, and aid calcium handling and membrane depolarization

Given their compatibility, we next determined how conductive scaffolds generate transcriptomic differences within hPSC-CMs. Principal component analysis (PCA) (Fig. 3a; left) shows clustering due to substrate, while the Euclidean distance matrix illustrates the increased dissimilarity between conductive and non-conductive scaffolds (Fig. 3a; right). Using an adjusted p-value (p-adj.) value of less than 0.05 and log fold change (FC) cut-off of 0.25, 287 differentially expressed genes (DEGs) were identified between the hPSC-CMs seeded on the PVA-only and PEDOT:PSS scaffolds (Fig. 3b, Table S1). Gene ontology (GO) terms associated with PVA-only scaffolds included response to external stimulus, immune system process, response to virus, and innate immune response, illustrating an increased stress response on PVA-only scaffolds. In contrast, the presence of PEDOT:PSS produced terms related to heart contraction, heart process, muscle system process, muscle contraction, and a decreased stress response (Fig. 3c, Table S2). We further plotted the normalized gene expression of cardiac genes related to these GO terms and found hPSC-CM contractility (*MYH6, MYH7, MYL7*), sarcomere organization (*TCAP*), and electrophysiology (*KCNIP2, ATP1A2, RNF207*) gene expression was elevated on conductive scaffolds (Fig. 3d). Given that *MYH7* is a marker of hPSC-CM maturity [36], these findings suggest that a conductive environment not only leads to increased contractility gene expression but may also result in additional maturation beyond protocols used to differentiate hPSC-CMs initially [15]. While the switch from *MYL7* to *MYL2* is another marker of maturity [36], *MYL2*, though not a DEG, has higher expression on hPSC-CMs on conductive scaffolds compared to PVA-only scaffolds (Table S3). Our results also indicated the upregulation of *TCAP,* which encodes for

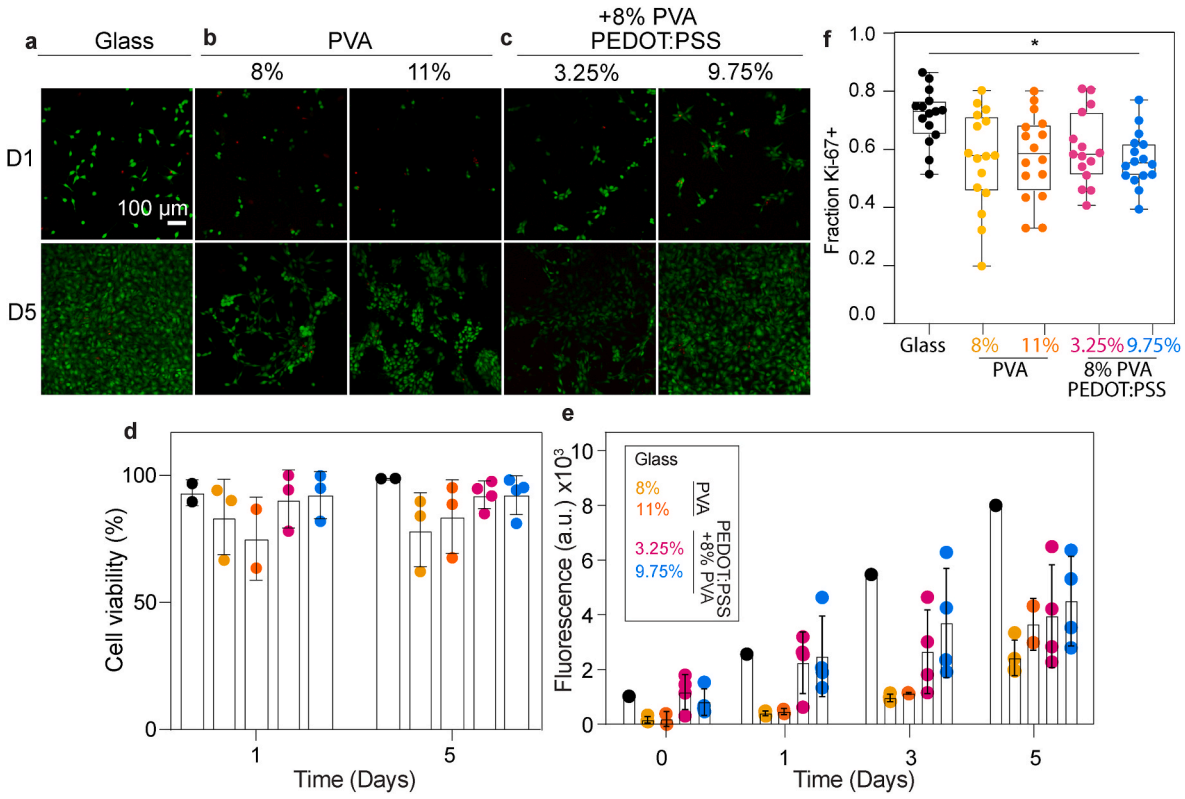

Fig. 2. Cells are viable and proliferative independent of PEDOT:PSS concentration. LIVE/DEAD staining 1 and 5 days after NIH/3T3 cell seeding on (a) glass, (b) 8 % and 11 % PVA, and (c) 8 % PVA scaffolds containing 3.25 % and 9.75 % PEDOT:PSS. Green indicates live cells and red indicates dead cells. Scale bars (a–c) = 100 μm. (d) Cell viability was calculated as the number of live cells over the total (live + dead) cells and represented as mean ± std dev. At day 5, cell viability is above 90 % for glass and electrospun scaffolds containing PEDOT:PSS. For D1, n = 2, 3, 2, 3, and 3 for glass, 8 % and 11 % PVA, and 8 % PVA scaffolds containing 3.25 % and 9.75 % PEDOT:PSS, respectively. For D5, n = 2, 3, 3, 4, and 4 for glass, 8 % and 11 % PVA, and 8 % PVA scaffolds containing 3.25 % and 9.75 % PEDOT:PSS, respectively. (e) Cell proliferation (mean ± std) as measured by resazurin fluorescence intensity illustrates higher cell viability with increasing PEDOT:PSS concentration as compared to PVA-only scaffolds. For D1, n = 1, 4, 2, 4, and 4 for glass, 8 % and 11 % PVA, and 8 % PVA scaffolds containing 3.25 % and 9.75 % PEDOT:PSS, respectively. For D5, n = 1, 4, 2, 4, and 4 for glass, 8 % and 11 % PVA, and 8 % PVA scaffolds containing 3.25 % and 9.75 % PEDOT:PSS, respectively. (f) The fraction of Ki67 positive cells is indicated in the plot at day 5 post-plating on the indicated scaffolds. Statistical significance was determined via a mixed-effects analysis for (d), a two-way ANOVA for (e), or a one-way ANOVA for (f), both with Tukey's multiple comparison test. (For interpretation of the references to colour in this figure legend, the reader is referred to the Web version of this article.)

titin-cap and enables titin assembly at the Z-disk [37], as well as electrophysiological genes on PEDOT:PSS/PVA scaffolds. Based on our transcriptomic analysis, we find that PEDOT:PSS/PVA scaffolds cause increased contractility, sarcomere, and electrophysiological gene expression, which may impact hPSC-CM function.

To assess the morphological and functional impact of the transcriptomic differences, we first looked at desmoplakin, which provides cardiac mechanical stability and aids in electrical communication through the maintenance of gap junctions [38,39]. After 3 days of exposure to experimental substrates, DP was highly localized to the hPSC-CM perimeters on conductive scaffolds compared to non-conductive scaffolds (Fig. 4a). Mean DP fluorescence intensity was similar between gelatin-coated glass and conductive scaffolds, indicating that similar DP expression for mechanical stability can be achieved on electrospun scaffolds even in the absence of native ECM components (Fig. 4b). Further, the differences between conductive and non-conductive scaffolds were statistically significant, illustrating that a conductive microenvironment aids in mechanical stability. In addition to DP, organized sarcomeres are necessary for the contractility of hPSC-CMs [40]. hPSC-CMs were seeded as either sub-confluent or confluent monolayers to determine if the conductive scaffolds could promote sarcomere organization in hPSC-CMs that are not directly in contact with one another. At both seeding densities, scaffolds containing PEDOT:PSS improved sarcomere organization index compared to PVA-only (Fig. 4c), when assessed via an unbiased organization index, which scaled with increasing PEDOT:PSS concentration even in the absence of a confluent monolayer (Fig. 4d); sarcomere organization differences were also indicative in overall morphology differences as a function of increasing PEDOT:PSS concentration (Fig. S2) and were not impacted by differences in CM purity between substrates (Fig. S3). These results suggest that the presence of PEDOT:PSS permits sarcomeres to organize in hPSC-CMs with or without a monolayer and integrin attachment points, further establishing the importance of a conductive scaffold for electrical signal propagation.

Intracellular calcium homeostasis involves the release and reuptake of calcium through various calcium handling machinery, resulting in subsequent contractions and force generation by sarcomeres [41,42]. Intercellular calcium, and therefore cell-cell electrical communication, is facilitated by gap junctions and allows for synchronous contractions of hPSC-CMs [43]. Thus, we investigated functional maturity through assessment of calcium handling kymographs in either the absence or presence of a confluent monolayer (Fig. 5a). For both cell densities, conductive scaffolds had more intense and frequent calcium spikes relative to 8 % PVA-only scaffolds (Fig. 5b); normalized fluorescent intensity (dF/F_0) was highest in the presence of PEDOT:PSS at both cell densities compared to all other substrates (Fig. 5c). This suggests that the presence of PEDOT:PSS allows for a larger calcium flux from the sarcoplasmic reticulum (SR) into the cytoplasm of hPSC-CMs [44], implying stronger contractions. In addition to dF/F_0, the time for each calcium cycle to peak decreased at both low and high seeding densities

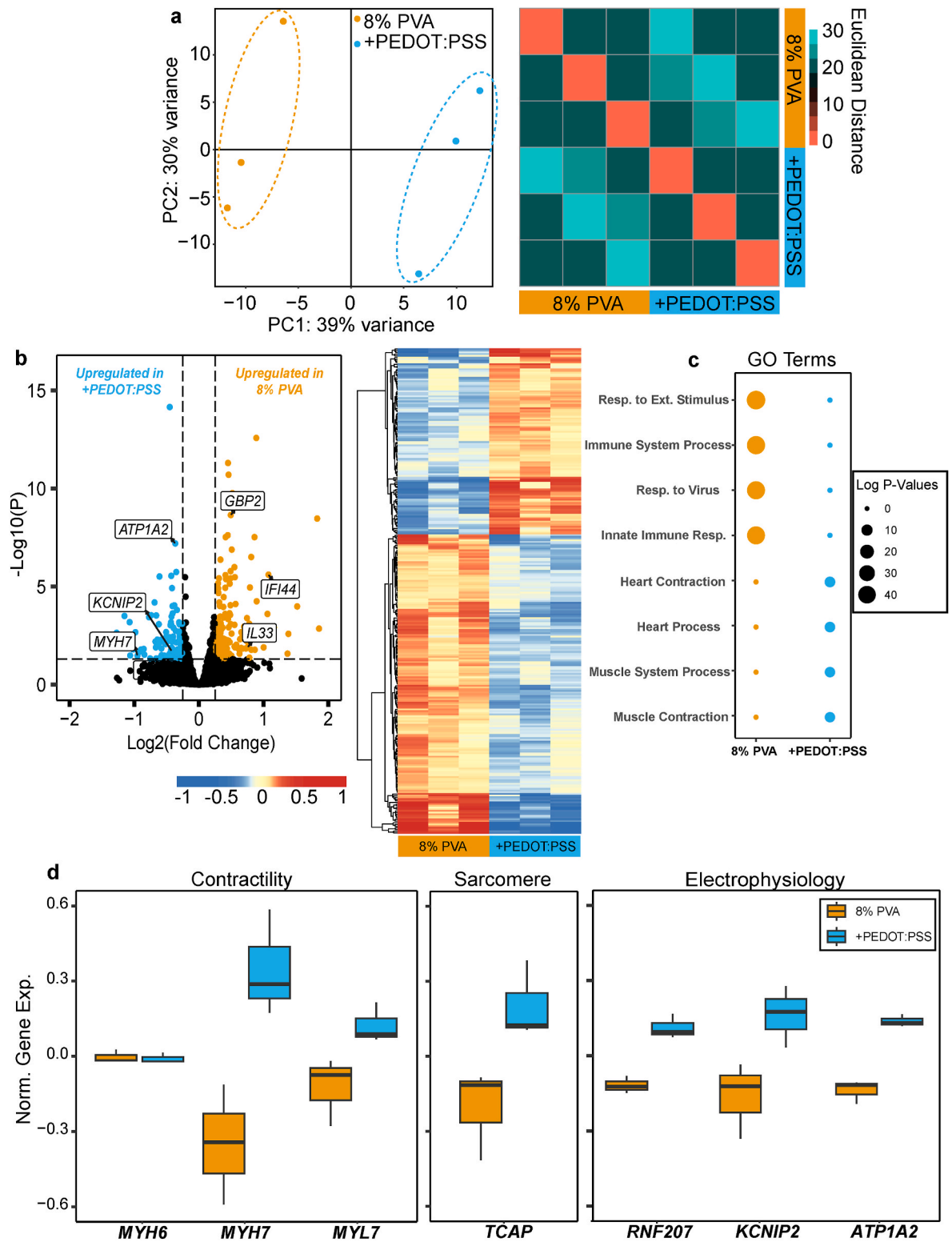

Fig. 3. RNA sequencing identifies upregulation of cardiac-related genes on conductive substrates. (a) PCA (post-batch correction) for hPSC-CMs seeded on 8 % PVA or 8 % PVA+9.75 % PEDOT:PSS scaffolds with total contribution from each axis noted (left) and Euclidian distance matrix (right) indicating the similarity between groups, where 30 indicates the largest dissimilarity between samples. (b) Volcano plot (left) indicating differences in DEGs between 8 % PVA and conductive scaffolds and heatmap (right) illustrating transcriptomic clustering of the top 287 significant genes. (c) Top four GO terms for each experimental condition and their statistical significance. (d) Normalized expression of genes related to hPSC-CM contractility, sarcomere organization, and electrophysiology (p-adj. < 0.05). A FC cut-off >0.25 and p-adj. cut-off <0.05 for (b) and (c) was used.

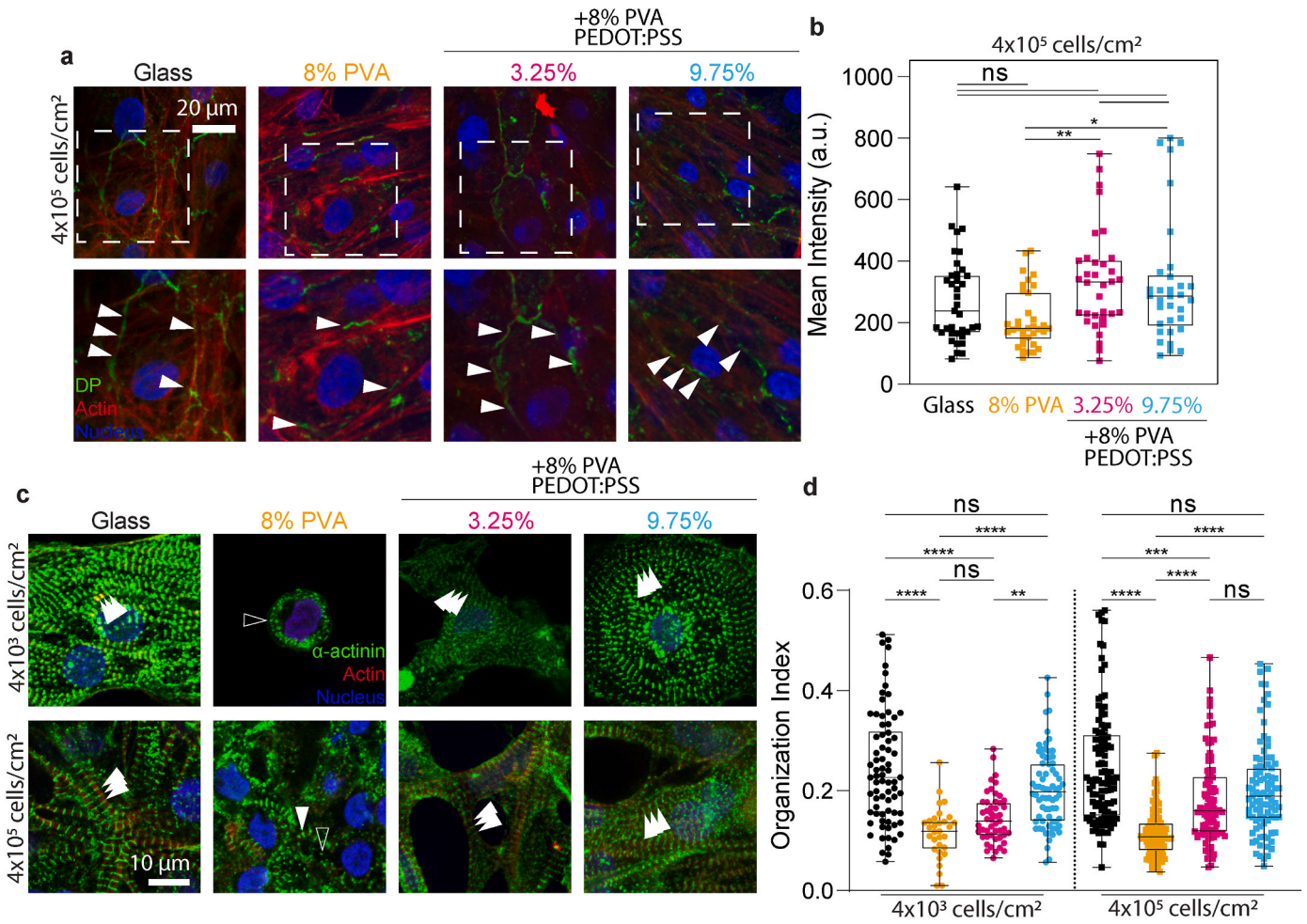

Fig. 4. Structural characterization of hPSC-CMs. (a) IF images of desmoplakin (DP) localization in hPSC-CMs seeded on glass, 8 % PVA, and PEDOT:PSS/PVA (3.25 % and 9.75 %) electrospun scaffolds at the indicated densities. Scale bar = 20 μm. (b) Mean DP pixel intensity is plotted for each condition. Data is reported as the mean pixel intensity of DP across four biological replicates with 5–11 images per sample. (c) IF images of hPSC-CMs seeded on glass, 8 % PVA, and PEDOT:PSS/PVA (3.25 % and 9.75 %) electrospun scaffolds at the indicated densities. Filled arrowheads indicate organized sarcomeres and open arrowheads indicate unorganized sarcomeres. Scale bar = 10 μm. (d) Sarcomere organization index is plotted for the indicated scaffold compositions on a scale of 0 (least) to 1 (most) organized. Each point represents one section of an image across three biological replicates. Statistical significance was determined via a one-way ANOVA with Tukey's multiple comparisons test (b) and Kruskal-Wallis test with Dunn's multiple comparisons (d) test to account for unequal variance between experimental groups.

on PEDOT:PSS compared to PVA-only scaffolds (Fig. 5d), demonstrating that conductive scaffolds enable rapid calcium efflux. Although cycle length and width (Fig. 5, e-f), which indicate how fast calcium is being taken into the SR, did not decrease with increasing PEDOT:PSS concentration in non-monolayer cells, both values decreased in the presence of a monolayer. Likewise, when comparing cycle length and width, there was density-dependent improvement in timing of hPSC-CMs seeded on the same substrate (Fig. 5, e-f). Thus, signal intensity is enhanced by conductivity through the presence of PEDOT:PSS whereas signal timing is enhanced by monolayer confluence.

To further probe the effect of conductive substrates on the cell retention and electrophysiology of hPSC-CMs over an extended period, i.e. 7 days of culture, we assessed action potential intensities and depolarization events of these cells seeded in monolayer on our substrates. After 7 days of culture, hPSC-CMs failed to form monolayers on 8 % PVA (Fig. 6a), while monolayers were maintained on all other conditions. Assessed kymographs (Fig. 6b) illustrate how decreased cell attachment on 8 % PVA resulted in asynchronous depolarization events, while the enhanced attachment to conductive scaffolds allowed for synchronicity across independent ROIs. Further, overall action potential intensity remained significantly higher on conductive substrates (Fig. 6c), similar to calcium flux experiments (Fig. 5c) performed after only 3 days of culture. This suggests that over time, the electrophysiological function, particularly signal intensity, remains higher across hPSC-CMs in the presence of PEDOT:PSS, and it may be supported through voltage-gated sodium channels such as Nav1.5 which is responsible for initial membrane depolarization [45]. Interestingly, the total percentage of depolarizing ROIs decreased on non-conductive substrates, i.e. glass and 8 % PVA scaffolds, compared to PEDOT:PSS scaffolds (Fig. 6d). Therefore, while cells experienced improved attachment to gelatin-coated glass compared to 8 % PVA, they experienced an almost identical percentage of depolarizing events, likely due to the lack of a conductive microenvironment to assist in signal propagation. Because of these differences in depolarization events, temporal parameters such as cycle length became difficult to interpret across different substrates. While 8 % PVA had similar cycle length to 9.75 % PEDOT:PSS scaffolds, the lower percentage of depolarizing ROIs and lack of monolayer made these comparison challenging as cell density affects action potentials in hPSC-CMs [46]. However as a function of PEDOT:PSS, cycle length decreased such that cells depolarized more often on 9.75 % PEDOT:PSS scaffolds. Taken together with calcium handling, these data demonstrate that PEDOT:PSS allows for higher calcium and action potential intensity as well as synchronicity in hPSC-CMs, both of which are illustrative of improved electrical maturity.

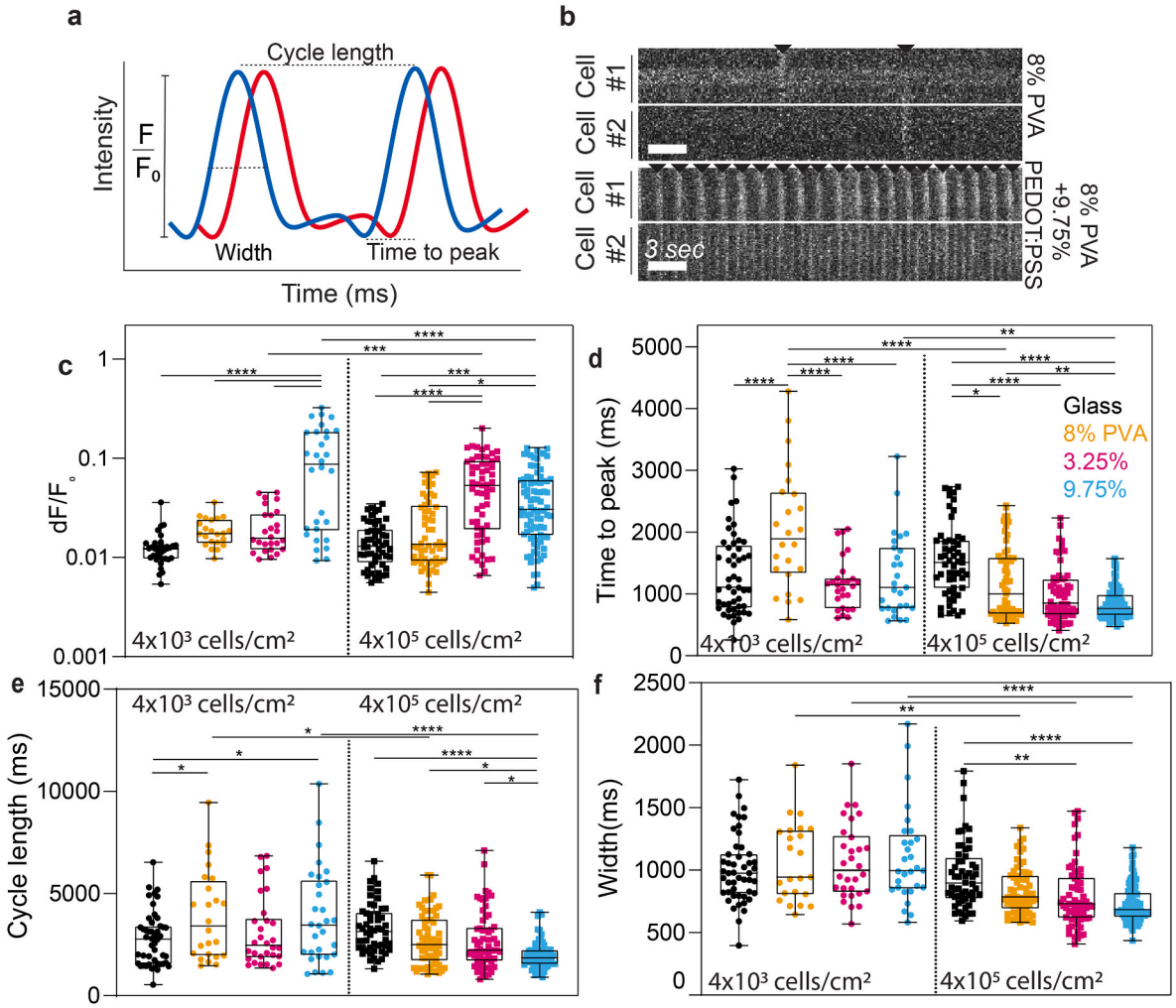

Fig. 5. hPSC-CM calcium handling on conductive PEDOT:PSS/PVA electrospun scaffolds. (a) Graphical illustration of relevant calcium handling parameters. (b) Kymograph of hPSC-CMs in monolayer on 8 % PVA or 9.75 % PEDOT:PSS/PVA. Black chevron indicates calcium peak. Scale = 3 s dF/F_o (c) increases and time to peak (d) decreases with increasing PEDOT:PSS concentration in both low and high hPSC-CM seeding densities. Cycle length (e) and width (f) decrease with increasing PEDOT:PSS concentration at high seeding densities. Each point represents one cell across n = 3 biological replicates. Statistical significance was determined by one-way ANOVA with Tukey's multiple comparison test.

4. Conclusion

Here we constructed composite PEDOT:PSS/PVA electrospun scaffolds to enhance the structural and functional maturity of hPSC-CMs in the absence of external stimuli. These scaffolds are biocompatible, capable of mimicking mechanical and physical properties of native cardiac tissue and provide a conductive microenvironment for electrical signal propagation. Initial transcriptomic analysis revealed upregulated cardiac genes in hPSC-CMs on conductive scaffolds, motivating further investigation of important structural protein organization and functionality. We found an increase in DP localization and sarcomere organization of hPSC-CMs in the conductive environment compared to an insulating (non-conductive) environment and, surprisingly, saw that sarcomere organization increased under these conditions even in the absence of a cell monolayer. Calcium handling experiments further revealed improved functional maturity of both low and high density hPSC-CMs on conductive scaffolds, indicated by increased calcium signal intensity and decreased time to peak. Upon investigating how these cells responded to PEDOT:PSS after a prolonged time in culture, we found improved cell retention, higher instances of depolarizing ROIs, and stronger action potential intensities on conductive substrates. While many groups have investigated the effects of conductive materials in hPSC-CM maturity, including the use of PEDOT:PSS [47], here, we have demonstrated that maturity can be achieved in the absence of external stimulation or a confluent monolayer if hPSC-CMs are provided with a conductive microenvironment. Taken together, these data suggest that conductive polymer platforms are capable of conducting electrical signals between distant hPSC-CMs, further warranting their investigation in 3D engineered tissue constructs or for application in disease modeling purposes.

CRediT authorship contribution statement

Gisselle Gonzalez: Conceptualization, Investigation, Writing – original draft, Visualization. **Aileena C. Nelson:** Resources, Methodology. **Alyssa R. Holman:** Methodology, Software. **Alexander J. Whitehead:** Investigation. **Erin LaMontagne:** Investigation. **Rachel Lian:** Investigation. **Ritwik Vatsyayan:** Methodology, Investigation. **Shadi A. Dayeh:** Writing – review & editing, Supervision. **Adam J. Engler:** Conceptualization, Writing – original draft, Supervision, Funding acquisition.

Declaration of competing interest

The authors declare the following financial interests/personal relationships which may be considered as potential competing interests:

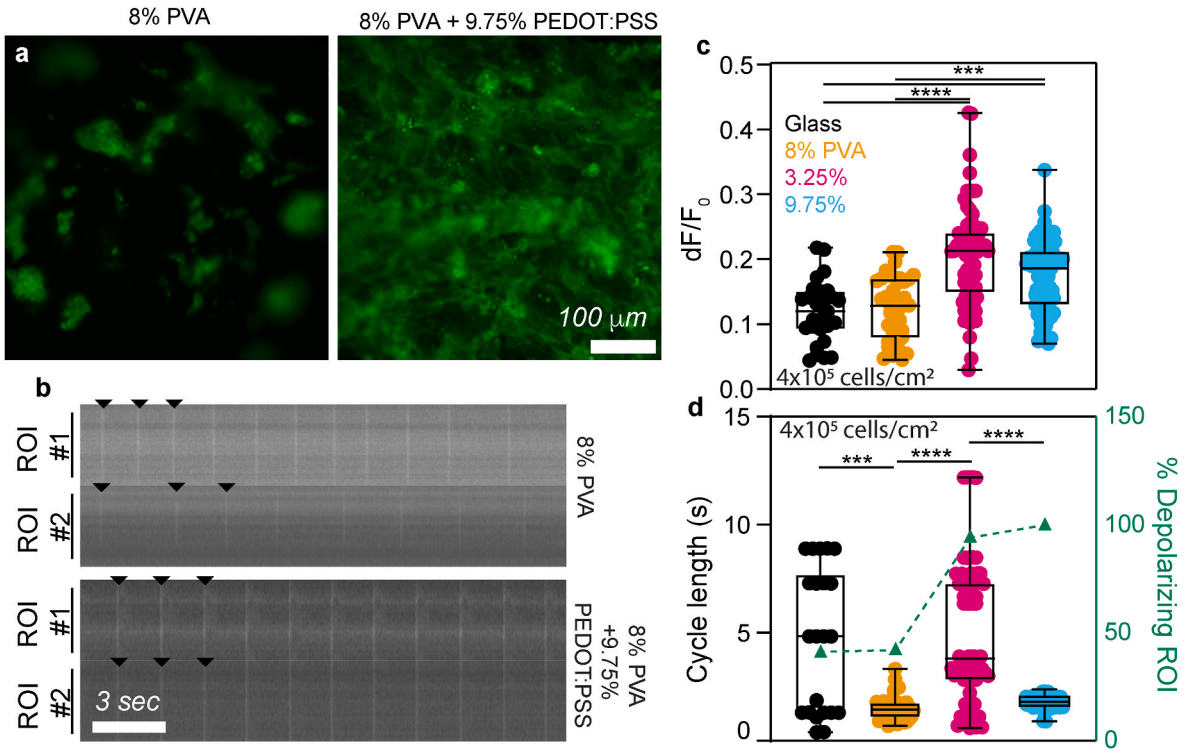

Fig. 6. hPSC-CM action potentials on conductive PEDOT:PSS/PVA electrospun scaffolds. (a) Representative images of hPSC-CMs seeded in monolayer and stained with voltage sensitive dye FluoVolt after 7 days of culture on 8 % PVA or 9.75 % PEDOT:PSS/PVA. Scale = 100 μm (b) Kymograph of hPSC-CMs ROIs on 8 % PVA or 9.75 % PEDOT:PSS/PVA. Black chevron indicates action potential peak. Scale = 3 s. (c) dF/F_o was measured on conductive scaffolds and plotted relative to glass and 8 % PVA. (d) Cycle length for rhythmically contracting cells was measured from kymographs and plotted. Since not all samples were rhythmically contracting, total percentage of depolarizing ROIs was also plotted (green) with the most number of depolarizing ROIs on conductive scaffolds (glass = 41.2 %; 8 % PVA = 42.3 %; 3.25 % = 94.4 %; 9.75 % = 100 %). Each point represents one ROI across n = 3 biological replicates. Statistical significance was determined by Kruskal-Wallis test with Dunn's multiple comparison test. (For interpretation of the references to colour in this figure legend, the reader is referred to the Web version of this article.)

Adam J. Engler, Shadi A. Dayeh, Alyssa R. Holman reports financial support was provided by National Institutes of Health. Aileena C. Nelson reports financial support was provided by American Heart Association Inc. Gisselle Gonzalez, Erin LaMontagne, Alexander J. Whitehead reports financial support was provided by National Science Foundation.

Data availability

Data will be made available on request.

Acknowledgements

The authors would like to thank Dr. Neil Chi (UCSD) for the donation of the RUES2 ESCs, Dr. Karen Christman (UCSD) for access to the BioTek plate reader, Dr. Kristen Jepsen of the Institute for Genomic Medicine (UCSD) for technical assistance with sequencing, and Dr. Elsa Molina (Sanford Consortium Stem Cell Core) for access and maintenance of the LSM 780 microscope. This work was performed in part at the San Diego Nanotechnology Infrastructure (SDNI) of UCSD, a member of the National Technology Coordinated Infrastructure (NNCI), which is supported by the National Science Foundation (ECCS-2025752). The authors acknowledge funding and equipment support from the National Institutes of Health (R01AG045428 to A.J.E. and DP2EB029757-01 to S. A.D.). Fellowship support was provided by the American Heart Association (20PRE35180060 to A.C.N.), the National Science Foundation (to G.G., E.L., and A.J.W.), the San Diego Fellowship (to G.G.), and the National Institutes of Health (F31 HL163996 to A.R.H.).

Appendix A. Supplementary data

Supplementary data to this article can be found online at https://doi.org/10.1016/j.biomaterials.2023.122363.

References

[1] M. Ghovvati, M. Kharaziha, R. Ardehali, N. Annabi, Recent advances in designing electroconductive biomaterials for cardiac tissue engineering, Adv. Healthcare Mater. 11 (2022), 2200055.
[2] C.-W. Hsiao, et al., Electrical coupling of isolated cardiomyocyte clusters grown on aligned conductive nanofibrous meshes for their synchronized beating, Biomaterials 34 (2013) 1063–1072.
[3] A. Mihic, et al., A conductive polymer hydrogel supports cell electrical signaling and improves cardiac function after implantation into myocardial infarct, Circulation 132 (2015) 772–784.
[4] A. Gelmi, et al., Direct mechanical stimulation of stem cells: a beating electromechanically active scaffold for cardiac tissue engineering, Adv. Healthcare Mater. 5 (2016) 1471–1480.
[5] J.H. Tsui, et al., Conductive silk–polypyrrole composite scaffolds with bioinspired nanotopographic cues for cardiac tissue engineering, J. Mater. Chem. B 6 (2018) 7185–7196.
[6] K. Roshanbinfar, et al., Nanofibrous composite with tailorable electrical and mechanical properties for cardiac tissue engineering, Adv. Funct. Mater. 30 (2020), 1908612.
[7] M. Solazzo, F.J. O'Brien, V. Nicolosi, M.G. Monaghan, The rationale and emergence of electroconductive biomaterial scaffolds in cardiac tissue engineering, APL Bioeng. 3 (2019), 041501.
[8] D. Mantione, I. Del Agua, A. Sanchez-Sanchez, D. Mecerreyes, Poly(3,4-ethylenedioxythiophene) (PEDOT) derivatives: innovative conductive polymers for bioelectronics, Polymers 9 (2017) 354.
[9] R.L. Keate, J. Tropp, C. Serna, J. Rivnay, A collagen-conducting polymer composite with enhanced chondrogenic potential, Cell. Mol. Bioeng. 14 (2021) 501–512.
[10] M. Solazzo, et al., PEDOT:PSS interfaces stabilised using a PEGylated crosslinker yield improved conductivity and biocompatibility, J. Mater. Chem. B 7 (2019) 4811–4820.
[11] A. Abedi, M. Hasanzadeh, L. Tayebi, Conductive nanofibrous Chitosan/PEDOT:PSS tissue engineering scaffolds, Mater. Chem. Phys. 237 (2019), 121882.

[12] G. Kaushik, A. Fuhrmann, A. Cammarato, A. Engler, J. In situ mechanical analysis of myofibrillar perturbation and aging on soft, bilayered Drosophila myocardium, Biophys. J. 101 (2011) 2629–2637.
[13] G.K. Reeves, H.B. Harrison, Obtaining the specific contact resistance from transmission line model measurements, IEEE Electron. Device Lett. 3 (1982) 111–113.
[14] H.H. Berger, Contact resistance and contact resistivity, J. Electrochem. Soc. 119 (1972) 507.
[15] X. Lian, et al., Directed cardiomyocyte differentiation from human pluripotent stem cells by modulating Wnt/β-catenin signaling under fully defined conditions, Nat. Protoc. 8 (2013) 162–175.
[16] Andrews, Simon. FastQC: A Quality Control Tool for High Throughput Sequence Data.
[17] A. Dobin, et al., STAR: ultrafast universal RNA-seq aligner, Bioinformatics 29 (2013) 15–21.
[18] Y. Liao, G.K. Smyth, W. Shi, featureCounts: an efficient general purpose program for assigning sequence reads to genomic features, Bioinformatics 30 (2014) 923–930.
[19] M.I. Love, W. Huber, S. Anders, Moderated estimation of fold change and dispersion for RNA-seq data with DESeq2, Genome Biol. 15 (2014) 550.
[20] K. EnhancedVolcano Blighe, Publication-ready Volcano Plots with Enhanced Colouring and Labeling, ENHANCEDVOLCANO, 2022, https://doi.org/10.18129/B9.BIOC.
[21] Alboukadel Kassambara, Ggpubr: 'ggplot2', Based Publication Ready Plots, 2022.
[22] U. Raudvere, et al., Profiler: a web server for functional enrichment analysis and conversions of gene lists (2019 update), Nucleic Acids Res. 47 (2019) W191–W198.
[23] M.D. Robinson, D.J. McCarthy, G.K. Smyth, edgeR: A Bioconductor package for differential expression analysis of digital gene expression data, Bioinformatics 26 (2010) 139–140.
[24] J.T. Leek, W.E. Johnson, H.S. Parker, A.E. Jaffe, J.D. Storey, The sva package for removing batch effects and other unwanted variation in high-throughput experiments, Bioinformatics 28 (2012) 882–883.
[25] H. Wickham, ggplot2: Elegant Graphics for Data Analysis, Springer International Publishing, Imprint: Springer, 2016, https://doi.org/10.1007/978-3-319-24277-4.
[26] Raivo Kolde, Pheatmap: Pretty Heatmaps, 2019.
[27] M.R. Salick, et al., The scanning gradient Fourier transform (SGFT) method for assessing sarcomere organization and alignment, J. Appl. Phys. 127 (2020), 194701.
[28] A.D. Doyle, N. Carvajal, A. Jin, K. Matsumoto, K.M. Yamada, Local 3D matrix microenvironment regulates cell migration through spatiotemporal dynamics of contractility-dependent adhesions, Nat. Commun. 6 (2015) 8720.
[29] A.J. Engler, S. Sen, H.L. Sweeney, D.E. Discher, Matrix elasticity directs stem cell lineage specification, Cell 126 (2006) 677–689.
[30] A.J. Engler, et al., Embryonic cardiomyocytes beat best on a matrix with heart-like elasticity: scar-like rigidity inhibits beating, J. Cell Sci. 121 (2008) 3794–3802.
[31] M.F. Berry, et al., Mesenchymal stem cell injection after myocardial infarction improves myocardial compliance, Am. J. Physiol. Heart Circ. Physiol. 290 (2006) H2196–H2203.
[32] I. Miccoli, F. Edler, H. Pfnür, C. Tegenkamp, The 100th anniversary of the four-point probe technique: the role of probe geometries in isotropic and anisotropic systems, J. Phys. Condens. Matter 27 (2015), 223201.
[33] A. Kotwal, Electrical stimulation alters protein adsorption and nerve cell interactions with electrically conducting biomaterials, Biomaterials 22 (2001) 1055–1064.
[34] F.F.F. Garrudo, et al., Production of blended poly(acrylonitrile): poly (ethylenedioxythiophene):poly(styrene sulfonate) electrospun fibers for neural applications, Polymers 15 (2023) 2760.
[35] M. Marzocchi, et al., Physical and electrochemical properties of PEDOT:PSS as a tool for controlling cell growth, ACS Appl. Mater. Interfaces 7 (2015) 17993–18003.
[36] E. Karbassi, et al., Cardiomyocyte maturation: advances in knowledge and implications for regenerative medicine, Nat. Rev. Cardiol. 17 (2020) 341–359.
[37] S. Zhang, P. Londhe, M. Zhang, J.K. Davie, Transcriptional analysis of the titin cap gene, Mol. Genet. Genom. 285 (2011) 261–272.
[38] J. Zhang, Y. Liang, W.H. Bradford, F. Desmosomes Sheikh, Emerging pathways and non-canonical functions in cardiac arrhythmias and disease, Biophys Rev 13 (2021) 697–706.
[39] C.Y. Kam, et al., Desmoplakin maintains gap junctions by inhibiting Ras/MAPK and lysosomal degradation of connexin-43, JCB (J. Cell Biol.) 217 (2018) 3219–3235.
[40] S.D. Lundy, W.-Z. Zhu, M. Regnier, M.A. Laflamme, Structural and functional maturation of cardiomyocytes derived from human pluripotent stem cells, Stem Cell. Dev. 22 (2013) 1991–2002.
[41] Q. Lou, A. Janardhan, I.R. Efimov, Remodeling of calcium handling in human heart failure, in: Md S. Islam (Ed.), Calcium Signaling, Springer Netherlands, 2012, pp. 740 1145–1174.
[42] D.A. Eisner, J.L. Caldwell, K. Kistamás, A.W. Trafford, Calcium and excitation-contraction coupling in the heart, Circ. Res. 121 (2017) 181–195.
[43] T. Toyofuku, et al., Intercellular calcium signaling via gap junction in connexin-43-transfected cells, J. Biol. Chem. 273 (1998) 1519–1528.
[44] S. Guatimosim, C. Guatimosim, L.-S. Song, Imaging calcium sparks in cardiac myocytes, in: H. Chiarini-Garcia, R.C.N. Melo (Eds.), Light Microscopy, 689, Humana Press, 2011, pp. 205–214.
[45] B.T. Priest, J.S. McDermott, Cardiac ion channels, Channels 9 (2015) 352–359.
[46] D.T.M. Du, N. Hellen, C. Kane, C.M.N. Terracciano, Action potential morphology of human induced pluripotent stem cell-derived cardiomyocytes does not predict cardiac chamber specificity and is dependent on cell density, Biophys. J. 108 (2015) 1–4.
[47] K. Roshanbinfar, et al., Electroconductive biohybrid hydrogel for enhanced maturation and beating properties of engineered cardiac tissues, Adv. Funct. Mater. 28 (2018), 1803951.